Chapter 4
Fabrication of Nanoporous Silicon by Ion Implantation

T.S. Kavetskyy and A.L. Stepanov

Abstract Ion implantation is an advanced new technological method for the fabrication of nanoporous silicon material with metal nanoparticles. The methodology of this technique is developed by Ag^+-ion implantation with an energy of 30 keV and a dose of $1.5 \cdot 10^{17}$ ion/cm^2 into a polished monocrystalline silicon substrate. By using Raman spectroscopy, SEM and AFM measurements it is found that amorphous layers of porous silicon (PSi) with an average size of the porous holes on the order of 150–180 nm, a depth of about 100 nm and a wall thickness of about 30–60 nm are formed on the Si surface as a result of ion irradiation. Ion implantation is also applied to locally modify the surface of Si to create periodic plasmonic PSi microstructures with Ag nanoparticles with a diameter of 5–10 nm. The results obtained clearly demonstrate how low-energy ions can be used for the fabrication of photonic microstructures on Si surfaces in a single-step process, similarly as it was recently done for Cu^+-ion implanted silica glass.

Keywords Ion implantation • Nanoporous silicon • Silver nanoparticles

4.1 Introduction

Porous silicon (PSi) is one of the most widely studied modern structured materials whose application in micro, nano, and optoelectronics, as well as in sensorics, biosensorics, and solar cells, is very promising [1]. Such PSi layers were first obtained in the mid-1950s at Bell Labs [2], but it were not seriously used until

T.S. Kavetskyy (✉)
Drohobych Ivan Franko State Pedagogical University, Drohobych 82100, Ukraine

John Paul II Catholic University of Lublin, Lublin 20-718, Poland
e-mail: kavetskyy@yahoo.com

A.L. Stepanov
Kazan Physical-Technical Institute of Russian Academy of Sciences, Kazan 420029, Russia

Kazan National Research Technological University, Kazan 420015, Russia

Kazan Federal University, Kazan 420008, Russia

© Springer Science+Business Media Dordrecht 2015

P. Petkov et al. (eds.), *Nanoscience Advances in CBRN Agents Detection, Information and Energy Security*, NATO Science for Peace and Security Series A: Chemistry and Biology, DOI 10.1007/978-94-017-9697-2_4

the discovery of their strong luminescent properties in 1990 [3]. Prior to this discovery, PSi was almost exclusively considered as insulating layer devices in the microelectronics industry. The detail advantages of PSi vs. silicon are observed in literature very well [4, 5]. Therefore, searching for new techniques to obtain PSi and improving the corresponding methods, existing for synthesis of such structures, is a topical problem now.

In the past, there were only two main technological methods for the production of PSi structures: electrochemical etching and chemical stain etching [4, 5]. Thus, PSi could be chemically created on silicon under appropriate conditions with porous sizes of a few nanometers to micrometers [1, 6]. Both the porosity and the pore morphology of PSi are greatly influenced by the electrochemical and chemical stain etching parameters such as temperature, current density, light illumination and so on.

The use of ion implantation with ions of rare gases to obtain nanodimensional PSi layers at the surface of monocrystalline silicon is also known. The solubility of rare gases in solids is very low and does not exceed a level of 10^{16} ions/cm^2. The gettering of gas bubbles from the matrix gas ions in irradiated polymer materials leads to the formation of nanopores (free volumes, nanovoids) [7]. In the case of silicon the implanted silicon wafers are subjected to thermal annealing in order to stimulate the nucleation and growth of pores from implanted gas ions [8]. This technique for the formation of pores at the surface of silicon was demonstrated earlier for implantation with ions such as He^+ [9], H^+ [10], Ne^+ [11], Ar^+ [12] and Kr^+ [11, 13].

Additionally, recently interest for silicon nanostructures containing noble metal nanoparticles has developed. It was initiated since metal nanoparticles with localized surface plasmon modes demonstrate a specific option to enhance the recombination rate of silicon light emitters to increase the efficiency of photoluminescence and internal quantum yield effectively, etc. [6, 14–16]. Silver nanoparticles (AgNPs) are the subject of increasing interest due to their strong plasmon resonance in the visible spectrum [17, 18]. For example, PSi samples coated with a layer of AgNPs showed after their electrochemical etching that the photoluminescence intensity remarkably increases [19], and the reflection of incident light with wavelengths below 1,100 nm can be reduced to use them for antireflection devices [20] or surface-enhanced Raman scattering of some organic molecules adsorbed on AgNP-PSi structures [15].

Instead of using simple silicon as the substrate for AgNPs deposition on the top of a sample, the ion implantation technique can be used to form AgNPs in the silicon volume as in the case of ion-irradiated silica glasses or polymers [18, 20–24]. Earlier, in experiments described [25, 26] Ag-ion implantation into crystalline silicon wafers and nanocrystalline silicon layers with an energy of 30–35 keV and a rather low dose of $5.0 \cdot 10^{15}$ ions/cm^2 was performed. Then AgNPs in the silicon matrix were synthesized after thermal annealing of the implanted samples at 500 °C. In another work [27], Ag^+-ion implantation of silicon using a conventional metal vapor vacuum arc (MEVVA ion source, which produces a mixture of Ag^{n+} ions) was applied with a higher dose of $2.0 \cdot 10^{17}$ ions/cm^2 to create AgNPs.

As will be discussed here and was shown in the literature [28], the physical technique of metal-ion implantation was not used before 2013 in practice for the fabrication of PSi [29]. A successful experiment of synthesis of PSi with implanted Ag nanoparticles was demonstrated, for the first time, in [29, 30]. A detailed description of the technological approach and new results obtained for AgNP-PSi structures are presented and explained in this contribution.

4.2 Experimental Procedure

Single crystalline p-type (100)-oriented silicon wafers were used as substrates for Ag^+-ion implantation to create PSi structures. Before implantation the substrates were cleaned by a wet chemical etching process. The silicon wafers were implanted with Ag^+ ions at the energy of 30 keV and an ion current density of 4 μA/cm^2 with doses in the range from $7.5{\cdot}10^{16}$ to $1.5{\cdot}10^{17}$ ions/cm^2 using the ion accelerate “ILU-3” at a residual pressure of 10^{-5} Torr and room temperature.

In an additional experiment, in order to reveal effects of sputtering or swelling of the surface, some silicon substrates were implanted through a mask consisting of a nickel mesh grid with square holes and a bar width of 20 μm. The mask was imposed onto the substrate during implantation to form a structure of irradiated and non-irradiated parts of the silicon surface. In this way, selectively implanted regions were prepared next to unimplanted ones in order to perform step-height profilimetry.

The depth distribution profiles of the Ag atoms and the damage level in the implanted silicon were modeled using the simulation-program “Stopping and Range of Ions in Matter” (SRIM-2013) [31].

The morphology of the implanted structured silicon surfaces were characterized in plan-view by scanning electron microscopy (SEM) using a high-resolution microscope (Merlin Carl Zeiss) combined with ASB (angle selective backscattering) and SE InLens (secondary electrons energy selective backscattering) detectors; in addition it was also equipped with a AZTEC X-MAX energy-dispersion spectrometer from Oxford Instruments for energy-dispersive X-ray spectroscopy (EDX) analysis.

The crystallinity of the implanted silicon structure was estimated from Raman spectra recorded with a DFS-52 spectrometer at room temperature, excited by a continuous argon laser LGN-502 with a wavelength of 448 nm and a radiation power of 50 mW.

Surface morphology observations and measurements of the profile and depth of pores (cross sections) in PSi were carried out by an Innova Bruker atomic-force microscope (AFM). A quantitative evaluation of the size of the pores was carried out by histograms with the size distribution using the Axio Vision computer software for processing SEM images according to the method described in [32].

The focused ion beam technique (FIB) was applied to provide milling of the implanted silicon surface for analyzing the sample depth by Auriga CrossBeam

Workstation Carl Ziess (FIB-SEM) with a 30 keV Ga liquid metal ion source at normal incidence. By this approach a square of $2 \times 2\ \mu m^2$ on a PSi surface was written with a ion current density of 50 nA/cm^2 that did not heat the sample but effectively sputtered the implanted surface.

4.3 Results and Discussion

4.3.1 Vacancies and Ion Depth Distribution

Ion implantation is a widely applied technique used for controlled in-depth doping of various metals, dielectrics, and semiconductors by embedding into them energetically accelerated ions of various chemical elements [1]. According to SRIM simulations, during ion bombardment a vacancy-rich region and an accumulation of implanted ions can be formed close to the surface in the irradiated matrix (Fig. 4.1). The mean penetration range R_p^{Ag} of 30 keV accelerated Ag^+-ions in a silicon substrate is about 26 nm with a longitudinal straggling ΔR_p^{Ag} of 8 nm with a Gaussian depth distribution (Fig. 4.1a). Thus, the predicted thickness of the modified silicon surface layer $R_p + 2\Delta R_p$ is about 42 nm.

Wang and Birtcher [33] assumed that during ion implantation porous structures in various semiconductors can result from nucleation of small voids in the irradiated materials by vacancy generation. Therefore the vacancy depth distribution for silicon implanted with Ag^+ ions was also simulated by SRIM (Fig. 4.1b), which shows a profile similar to the ion distribution for such low energies. Analyzing the SRIM modeling, however, should take in account that the depth distribution of Ag-ions and vacancies obtained correspond to an implantation process in an

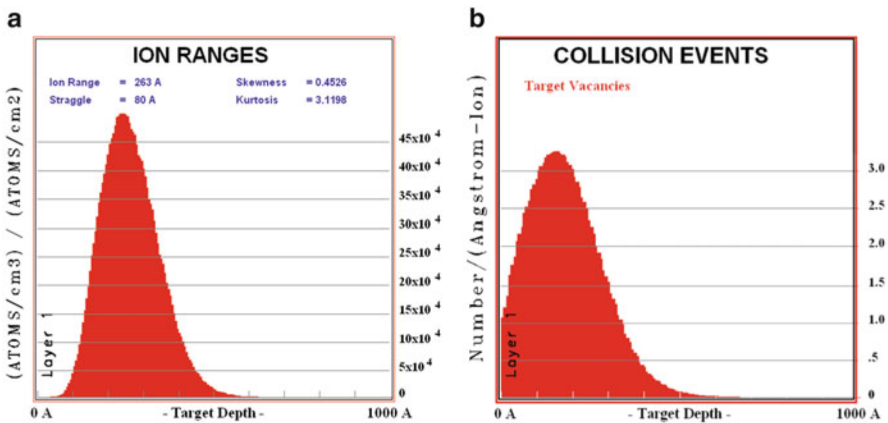

Fig. 4.1 Depth ion distribution of Ag-ions implanted (**a**) and generated vacancy profiles (**b**) in silicon with energy of 30 keV calculated using the SRIM code

uniform silicon matrix before nucleation and growth of PSi (for ion doses less than $1.0 \cdot 10^{16}$ ions/cm^2). As will be shown below, a prolonged irradiation results, simultaneous with the formation of PSi and the segregation of silver near the surface, in silicon sputtering.

4.3.2 SEM Study of PSi Structure

Figure 4.2a shows a plane-view SEM image of unimplanted silicon, which looks very smooth without any surface structural inhomogeneity.

The results of the creation of pores on the silicon samples are observed by plan-view SEM images (Fig. 4.3). In contrast to unimplanted silicon (Fig. 4.2) the characteristic PSi surface structures show the appearance of black holes in the implanted silicon region. They consist of nearly cellular features separated by rather thin walls with thicknesses about 30–60 nm. Such features are clearly resolved for all samples formed by various Ag-ion dose irradiations: $7.5 \cdot 10^{16}$, $1.0 \cdot 10^{17}$ and $1.5 \cdot 10^{17}$ ions/cm^2. Uniform pore distributions with distinguished sharp holes were observed for all implanted surfaces on silicon-implanted samples. The size of the pores was measured by counting the number of holes in several micrographs, taking into account all visible holes boundaries and subtracting those holes that intersects an edge of the SEM image. From this, the size of the pores was estimated. It can be seen that mean pore size (black holes) increase in magnitude with increasing Ag-ion doses. White spots in these SEM figures correspond to a material with a higher density compared to silicon which suggests them to be AgNPs.

Figures 4.2b and 4.4 present EDX spectra recorded on the examined unimplanted silicon and on PSi structures with AgNPs fabricated with the highest

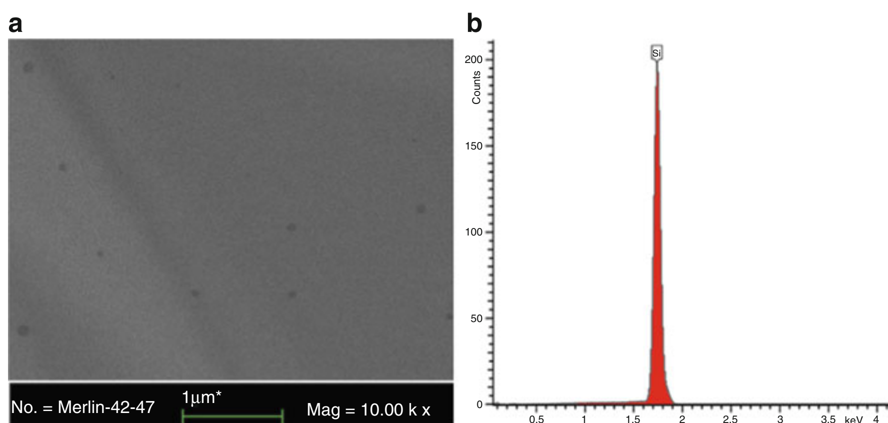

Fig. 4.2 SEM image (**a**) and EDX characteristic spectrum (**b**) of unimplanted silicon

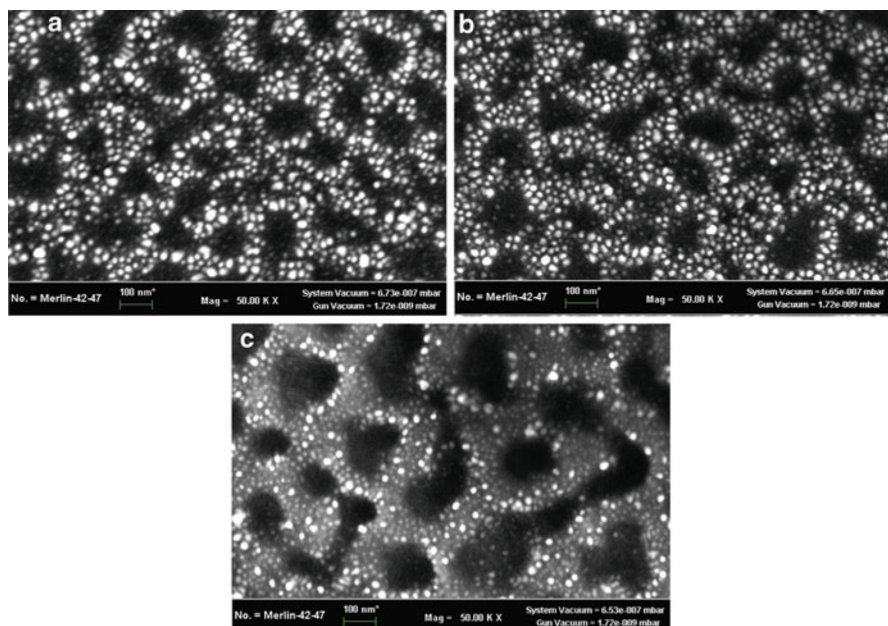

Fig. 4.3 SEM images of PSi fabricated by Ag^{+}-ion implantation into silicon with various doses: (**a**) $7.5{\cdot}10^{16}$; (**b**) $1.0{\cdot}10^{17}$ and (**c**) $1.5{\cdot}10^{17}$ ions/cm^2

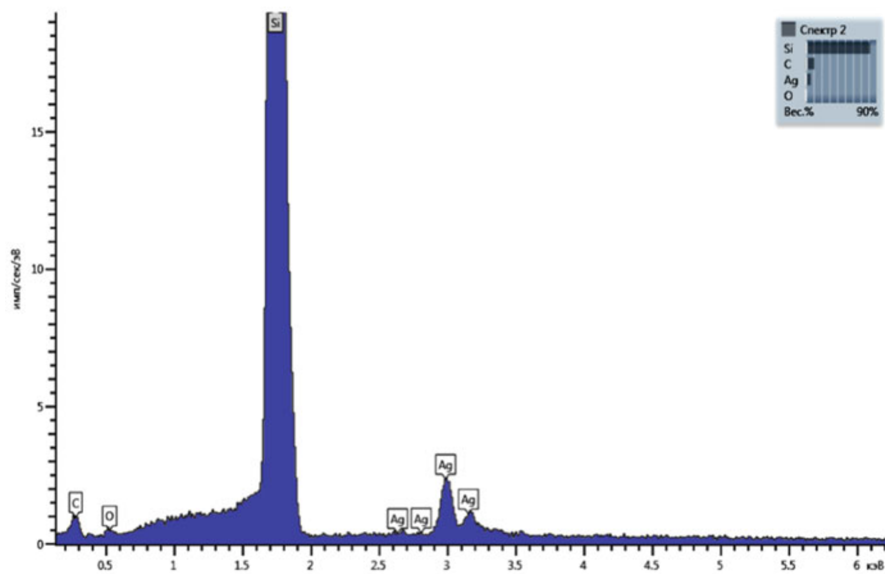

Fig. 4.4 EDX characteristic spectrum of PSi fabricated with an ion dose of $1.5{\cdot}10^{17}$ ions/cm^2. The visible EDX peaks confirm the presence of Ag in the synthesized PSi structures

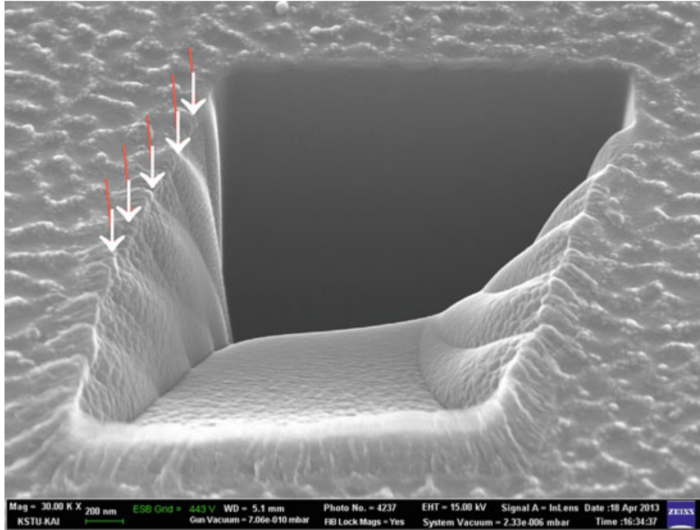

Fig. 4.5 SEM image of a sample surface with PSi structures (as in Fig. 4.3a) fabricated with an Ag^+-ion dose of $1.5 \cdot 10^{17}$ ions/cm^2 after FIB treatment with Ga ions. The *arrows* show the top positions of vertically continued structures on the walls of the FIB-milled cross-section

ion dose, respectively. Such EDX spectra for implanted samples were recorded in the surface area outside the black holes of the silicon pores. In contrast to the EDX data for unimplanted silicon, in the middle part of the presented spectrum of PSi four peaks located between 2.5 and 3.5 keV are clearly seen. These maxima are characteristic for Ag. It was observed that the intensity of the EDX Ag peaks increases with increasing implantation dose which means a growing Ag concentration in the silicon samples. The appearance of Ag peaks is in consistence with the white spots in the SEM images of the PSi (Fig. 4.3), which correspond to AgNPs synthesized in PSi during ion implantation. As shown in the present study, using selected conditions for low-energy Ag-ion irradiation of silicon, AgNPs can be fabricated without post-implantation thermal annealing, which was earlier done in [25, 26].

For the applied FIB conditions of PSi treatment, the mean penetration depth of Ga^+-ions implanted into silicon was obtained by SRIM calculation, which gives a value $R_p^{Ga} = 28$ nm with a straggling ΔR_p^{Ga} of 10 nm in the Gaussian depth distribution. Figure 4.5 shows a SEM image of a FIB-milled cross-section of an irradiated area of the surface with PSi from Fig. 4.3c. The whole thickness of the affected layer is about 1 μm. On the walls short columnar structures (shown by arrows) with an approximate size of several tens of nanometers could be recognized, which is expends from the surface to the depth of the sample.

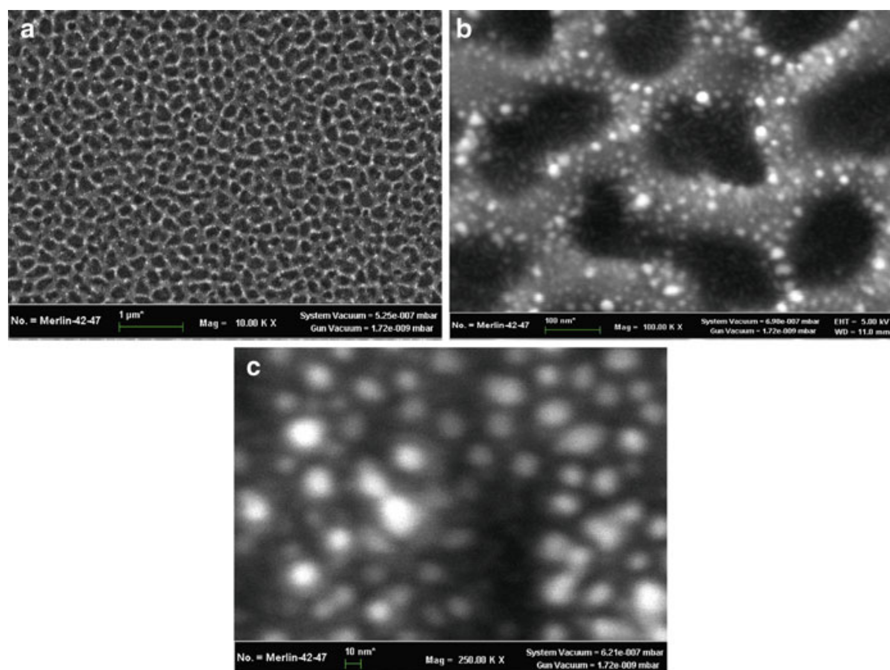

Fig. 4.6 SEM images of a PSi structure fabricated with a dose of $1.5 \cdot 10^{17}$ ions/cm^2 presented with different scales: (**a**) 1 μm; (**b**) 100 nm; (**c**) 10 nm

Figure 4.6 shows SEM images with various scales of the silicon surface implanted with silver ions. In contrast to the initial polished substrate, the morphology of the irradiated silicon surface is determined by the typical PSi structure. As can be seen from Fig. 4.6a, the PSi layer formed by implantation looks very homogeneous on a rather large scale (tens of microns). Reducing the scale (Fig. 4.6b) allows to estimate the average diameter of the pore holes (black in the image) to about 150–180 nm, as follows from the histogram of the pore size distribution presented in Fig. 4.7. The thickness of pore walls is estimated to be on the order of 30–60 nm. A further decrease of the scale (Fig. 4.6c) indicates the formation of implantation nanoinclusions (white) in the structure of the PSi walls with an average size on the order of ~5–10 nm. Since heavier chemical elements recorded by the detector of backscattered electrons are shown in the SEM microphotographs in a lighter tone, for a composite material composed of silicon atoms and implanted silver, it is possible to conclude that the white regions observed on a dark background (signals from silicon) are due to metallic silver in the form of nanoparticles (Fig. 4.6c). In this case it should be noted that silver atoms do not form any chemical compounds with silicon, similar to silicides of metals (cobalt, iron, etc.).

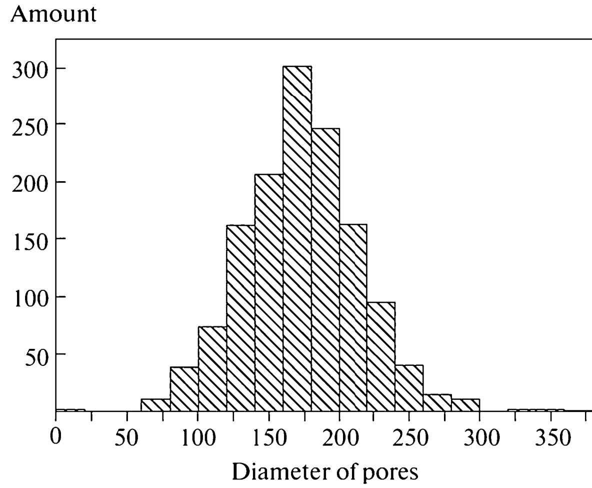

Fig. 4.7 Histogram of the pore size distribution in a PSi structure (Fig. 4.6b) formed by implantation of silicon with silver ions

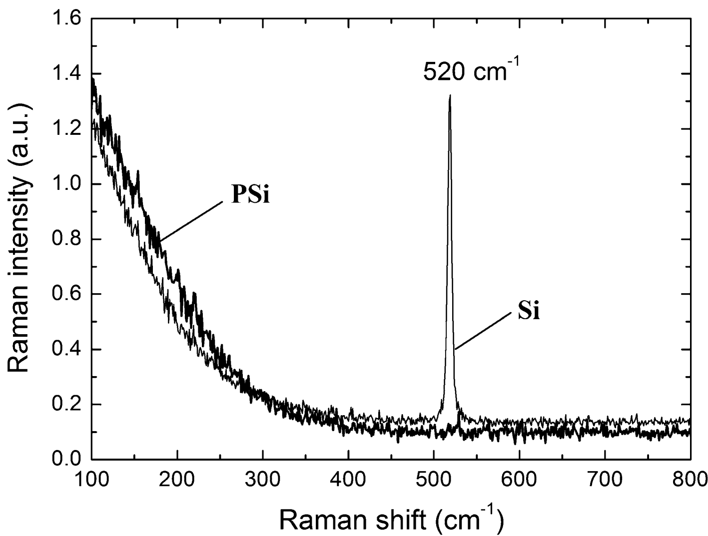

Fig. 4.8 Raman spectra of a polished monocrystalline Si substrate and a PSi structure fabricated at a dose of $1.5 \cdot 10^{17}$ ions/cm^2

Figure 4.8 shows Raman spectra of the polished monocrystalline Si substrate and a PSi structure fabricated with a dose of $1.5 \cdot 10^{17}$ ions/cm^2. By using Raman measurements of Ag^+-irradiated and non-irradiated silicon, it is demonstrated that the peak at a frequency of ~520 cm^{-1}, associated with scattering of optical phonons in the crystalline silicon matrix [34], disappears after ion implantation completely, thus characterizing the formed PSi layer as amorphous [35].

4.3.3 AFM Study of PSi Formation

Additional information proving the formation of PSi by implantation of silicon with Ag ions was obtained by AFM measurements. Figure 4.9a shows the AFM image observed from a fragment of the PSi surface, looking typically for porous structures in the case of AFM experiments [13]. Figure 4.9b gives the profiles of cross sections of individual pores measured in the directions shown in Fig. 4.9a, they allow an estimation of the depth of pores amounting to a value on the order of 100 nm. Thus, we can conclude that, as a result of silicon implantation with silver ions, characteristic pores are formed comparable with the relatively shallow pores in PSi obtained by an electrochemical method in highly diluted solutions of hydrofluoric acid [4].

4.3.4 PSi Structure Fabricated Through Mask

In order to estimate the steps formed at the interface between irradiated and non-irradiated regions of silicon by surface swelling or its sputtering during the ion implantation, in particular by the formation of pores in semiconductors, for example in germanium by irradiation with germanium ions, implantation through a mask is commonly suggested [28]. The formation of periodic plasmonic microstructures with metal nanoparticles with a diameter of 5–10 nm due to low-energy ion implantation in a single-step process was recently demonstrated in the case of Cu^{+}-ion implanted silica glass with different sizes of the grid mask [36, 37].

SEM images of a silicon surface containing fragments of PSi microstructures formed in this work by implantation with silver ions with a dose of $1.5 \cdot 10^{17}$ ions/cm^2 through a mask are shown in Fig. 4.10. As can be seen from the Fig. 4.10a, b, rectangular light-gray PSi regions were formed at the surface of silicon as a result of the implantation, which were confined by dark strips of non-irradiated crystalline silicon. A 3D reconstruction of a part of the sample close to an edge of the mask is presented in Fig. 4.10c, giving direct evidence for sputtering of the Ag^{+}-ion implanted silicon surface. In a first approximation, it can be speculated that the volume expansion is related to a mechanism simply governed by the nuclear energy deposition, which is usually measured in displacements per atom [33]. An AFM image of a fragment of a sample comprising a region of several square holes of the mask in 3D projection is shown in Fig. 4.11. As can also be seen from these figures, an efficient sputtering of the silicon-substrate surface takes place during the implantation of silicon with silver ions and the formation of a porous structure. Earlier, sputtering and erosion of silicon surfaces were observed by their irradiation with argon ions in an energy range of 50–140 keV [38]. However, there was no information about the formation of pores in this publication. As a result of implantation with Ag ions, holes and steps are formed at the interface between silicon and PSi in the irradiated part of silicon.

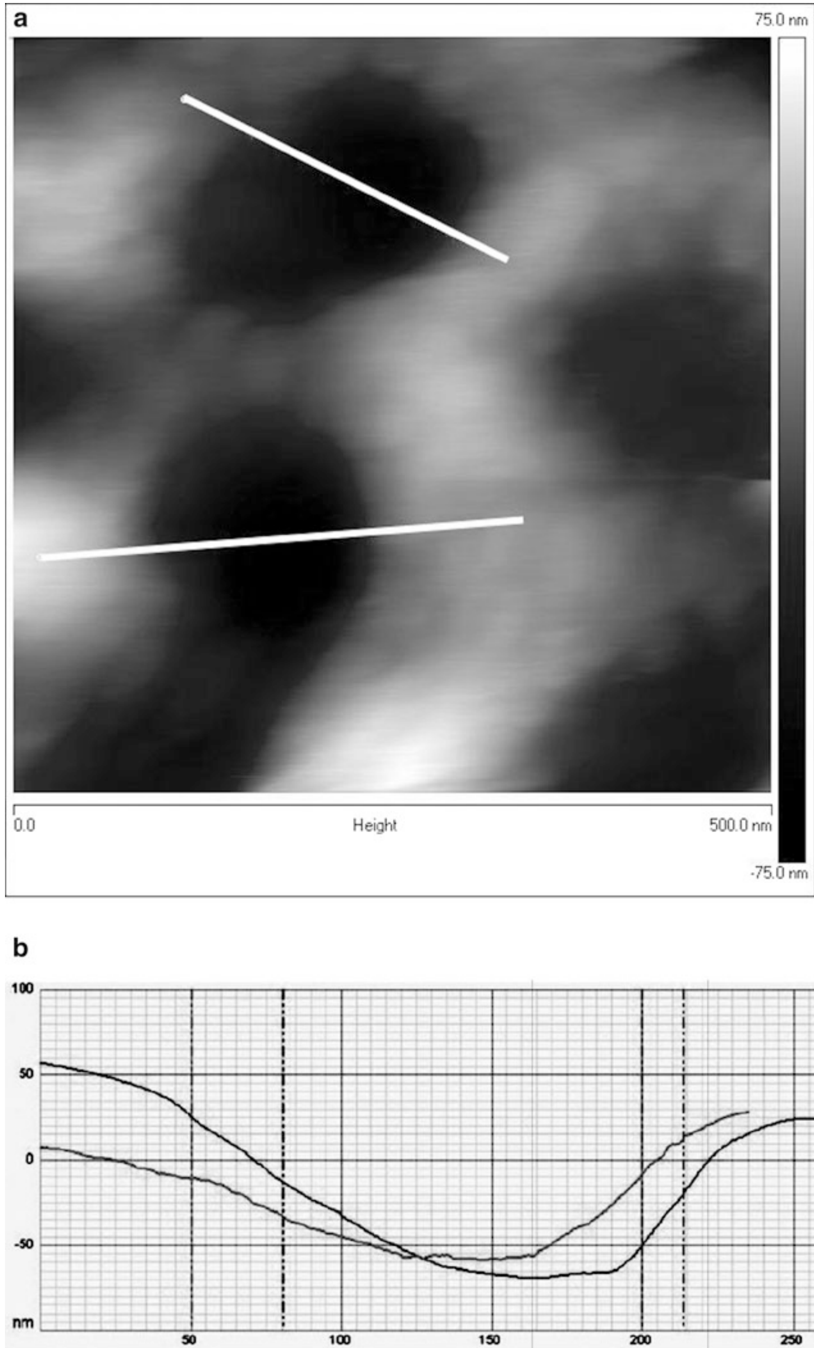

Fig. 4.9 (**a**) AFM images of the PSi surface obtained by silicon implantation with Ag ions and (**b**) profiles of individual pores measured on the directions shown in (**a**)

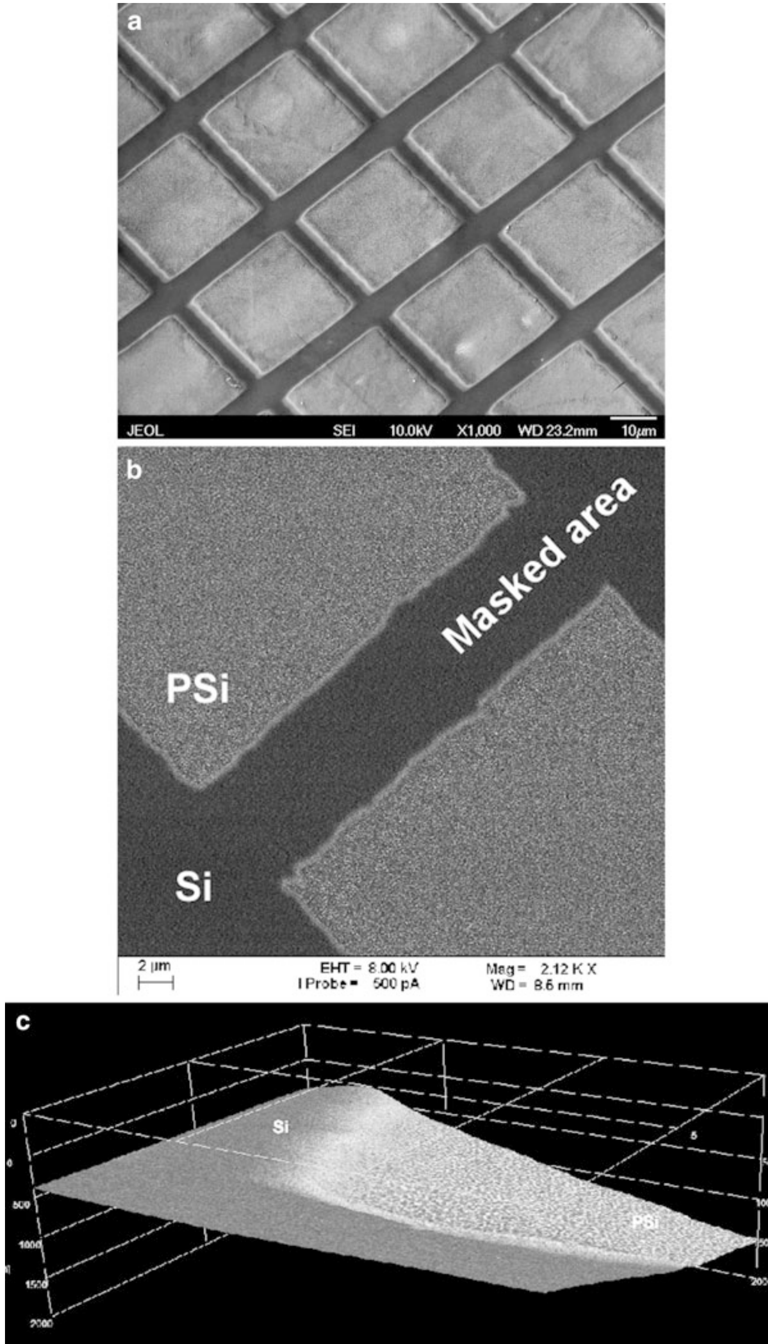

Fig. 4.10 (**a**) and (**b**) SEM images (with different scales) of structures with PSi (*light gray*) fabricated with an Ag^{+}-ion dose of $1.5{\cdot}10^{17}$ ions/cm^2 through a nickel mesh mask. (**c**) 3D SEM reconstruction of a step area that demonstrating sputtering of the silicon surface during Ag-ion implantation

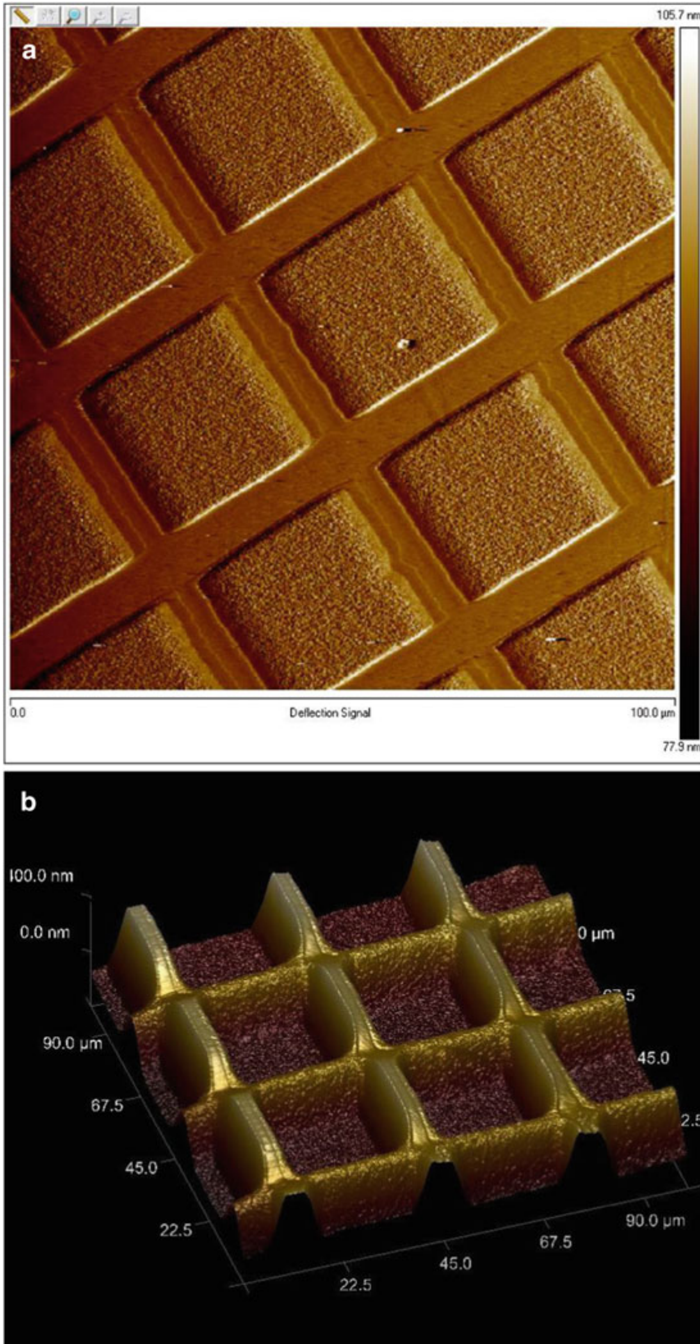

Fig. 4.11 (**a**) and (**b**) 3D fragments of an AFM image of the surface in the mask region, which demonstrates the sputtering of silicon

It is known that for a critical, rather low implantation dose, silicon undergoes a phase transition from a crystalline to the amorphous [39, 40]. As seen from the results reported in this work, at higher doses the amorphous silicon layer transforms to a porous structure with AgNPs. Thus, for the first time in practice it is demonstrated by the present experiments that PSi growth is stimulated by high-dose metal-ion implantation. This new result for silicon can be considered to be consistent with published data for porous semiconductors, in particular for germanium fabricated during an ion implantation process [28, 41–43] and, thus, a similar suited possible method for PSi structuring can be considered also. Sputtering effects (Figs. 4.10 and 4.11) seem to be important to determine the mechanism of PSi formation; this is somewhat unexpected, since it is known that by formation of pores in implanted semiconductors (germanium), an opposite phenomenon was observed: the swelling of the surface [28]. Therefore, the proposed mechanism of pore formation in implanted germanium based on the generation of vacancies in the irradiated semiconductor, which join the pores, cannot be merely transferred to the matrix of Si implanted with silver ions.

Despite PSi creation by metal-ion implantation of silicon, in the case of germanium there was a great debate over the past 30 years regarding the mechanisms governing the formation of porous semiconductor structures in ion-implanted germanium [44]. Currently, there are two main theories of void formation for germanium: vacancy clustering and the so-called “microexplosions”. The vacancy clustering theory involves an inefficient recombination of germanium point defects during ion implantation, where, once a critical point defect density is created by ion implantation, excess vacancies cluster into pores in order to minimize the dangling bond density. In contrast, the microexplosion theory is based on the creation of voids through pressure waves and thermal spikes caused by the overlap of ion cascades [44].

Therefore, in principle, it is possible to determine which theory better models the formation of voids and pores in silicon by selecting appropriate implant conditions and observing the resulting microstructure after ion implantation.

4.4 Conclusions

In this work a completely new technique used to obtain PSi layers with silver nanoparticles at the surface of monocrystalline silicon by a low-energy high-dose implantation was demonstrated. Ion implantation is one of the basic techniques used in industrial semiconductor microelectronics for the formation of various types of silicon nano- and microdevices. Therefore, the proposed new physical technique for the formation of PSi, in contrast to the well-known chemical approaches, has the advantage of being rather easily integrated into a modern industrial process for improving the technologies of the fabrication of microcircuits.

As follows from the results presented in this work, in our experiments PSi structures with silver nanoparticles were successfully obtained without a chemical technique in solution. Evidently, the further steps in improving this type of composite materials must consist of an optimization of the fabrication processes and, in particular, searching for correlation features between structural parameters and the characteristics of optical, plasmon, photoluminescence, and sensor properties of the new porous structures.

Acknowledgments T.S. Kavetskyy acknowledges the SAIA (Slovak Academic Information Agency) for scholarships in the Institute of Physics, Slovak Academy of Sciences within the National Scholarship Program of the Slovak Republic. A.L. Stepanov thanks for financial support by the Russian Scientific Foundation (No. 14-13-00758). This work was also partly supported by the State Fund for Fundamental Researches of Ukraine (No. F52.2/003). The authors are grateful to V.I. Nuzhdin and V.F. Valeev for help with the ion implantation procedure.

References

1. Torres-Costa V, Martin-Palma RJ (2010) J Mater Sci 45:2823
2. Uglir A (1956) Bell Syst Tech J 35:333
3. Canham LT (1990) Appl Phys Lett 57:1046
4. Feng ZC, Tsu R (1994) Porous silicon. World Scientific Publications, New York
5. Sallor MJ (2011) Porous silicon in practice. Willey-VCH, Weinheim
6. Oskam G, Long JG, Natarajan A, Searson PC (1998) J Phys D Appl Phys 31:1927
7. Kavetskyy T, Tsmots V, Kinomura A, Kobayashi Y, Suzuki R, Mohamed HFM, Šauša O, Nuzhdin V, Valeev V, Stepanov AL (2014) J Phys Chem B 118:4194
8. Kozlovskii VV, Kozlov VA, Lomasov VN (2000) Semiconductors 34:123
9. Stein HJ, Myers SM, Follstaedt DM (1993) J Appl Phys 73:2755
10. Cerofolini GF, Meda L, Balboni R, Corni F, Frabboni S, Ottaviani G, Tonini R, Anderle M, Canteri R (1992) Phys Rev B 46:2061
11. Wittmer M, Roth J, Revesz P, Mayer JM (1978) J Appl Phys 49:5207
12. Revesz P, Wittmer M, Roth J, Mayer JM (1978) J Appl Phys 49:5199
13. Galyautdinov MF, Kurbatova NV, Buinova EY, Shtyrkov EI, Bukharaev AA (1997) Semiconductors 31:970
14. Amran TS, Hashim MR, Al-Obaidi NK, Yazid H, Adnan R (2013) Nanoscale Res Lett 8:35
15. Chan S, Kwon S, Koo T-W, Lee LP, Berlin AA (2003) Adv Mater 15:1595
16. Wang M, Wang X, Ghoshal S (2013) Micro & Nano Lett 8:465
17. Kreibig U, Vollmer M (1995) Optical properties of metal clusters. Springer, Berlin
18. Stepanov AL (2010) Ion-synthesis of silver nanoparticles and their optical properties. Nova Scientific Publications, New York
19. Cao DT, Ngan LTQ, Anh CT (2013) Surf Interface Anal 45:762
20. Wang Y, Liu YP, Liang HL, Mei ZX, Du XL (2013) Phys Chem Chem Phys 15:2345
21. Ganeev RA, Ryasnyansky AI, Stepanov AL, Usmanov T (2004) Phys Status Solidi B 241:R1
22. Stepanov AL, Abdullin SN, Petukhov VY, Osin YN, Khaibullin IB (2000) Philos Mag B 80:23
23. Stepanov AL, Popok VN (2004) Surf Sci 566:1250
24. Stepanov AL (2010) Rev Adv Mater Sci 26:1
25. Sing AK, Gryczynski KG, McDaniel FD, Park SY, Kim M, Neogi A (2010) Appl Phys Express 3:102201
26. Sing AK, Gryczynski KG, Neogi A (2012) Opt Mater Express 2:501

27. Seo HW, Chen QY, Rusakova IA, Zhang ZH, Wijesundera D, Yeh SW, Wang XM, Tu LW, Ho NJ, Wu YG, Zhang HX, Chu WK (2012) Nucl Instrum Methods Phys Res B 292:50
28. Romano L, Impellizzeri G, Tomasello MV, Giannazzo F, Spinella C, Grimaldi MG (2010) J Appl Phys 107:84310
29. Stepanov AL, Trifonov AA, Osin YN, Valeev VF, Nuzhdin VI (2013) Optoelectron Adv Mater Rapid Commun 7:692
30. Stepanov AL, Osin YN, Trifonov AA, Valeev VF, Nuzhdin VI (2014) Nanotechnol Russia 9:163
31. Ziegler JF, Biersack JP, Littmark U (1985) The stopping and range of ions in solids. Pergamon Press, New York. http://www.srim.org/
32. Peckham J, Andrews GT (2013) Semicond Sci Technol 28:105027
33. Wang LM, Birtcher RC (1989) Appl Phys Lett 55:2494
34. Tyschenko IE, Popov VP, Talochkin AB, Gutakovskii AK, Zhuravlev KS (2004) Semiconductors 38:107
35. Trifonov AA, Osin YN, Valeev VF, Nuzhdin VI, Kavetskyy TS, Stepanov AL (2013) Nanotekhnologii: Nauka i Proizvodstvo 4(25):46
36. Stepanov AL, Evlyukhin EA, Nuzhdin VI, Valeev VF, Osin YN, Evlyukhin AB, Kiyan R, Kavetskyy TS, Chichkov BN (2013) Appl Phys A Mater Sci Process 111:261
37. Kavetskyy TS, Galyautdinov MF, Valeev VF, Nuzhdin VI, Osin YN, Evlyukhin AB, Stepanov AL (2013) Tech Phys Lett 39:591
38. Chini TK, Sanyal MK, Bhattacharyya SR (2002) Phys Rev B 66:153404
39. Chason E, Picraux ST, Poate JM, Borland JO, Current MI, Diaz de la Rubia T, Eaglesham DJ, Holland OW, Law ME, Mayer CW, Melngails J, Tasch AF (1997) J Appl Phys 81:6513
40. Williams JS (1998) Mater Sci Eng A 253:8
41. Romano L, Impellizzeri G, Bosco L, Ruffino F, Miritello M, Grimaldi G (2012) J Appl Phys 111:113515
42. Donovan TM, Heinemann K (1971) Phys Rev Lett 27:1794
43. Steinbach T, Wemecke J, Kluth P, Ridgway MC, Wesch W (1987) Phys Rev B 35:104108
44. Darby BL, Yates BR, Rudawski NG, Jones KS, Kontandos A, Elliman RG (2011) Thin Solid Films 519:5962